A Fluid Dynamic Based Coordination of a Wireless Sensor Network of Unmanned Aerial Vehicles: 3-D Simulation and Wireless Communication Characterization

Apratim Shaw and Kamran Mohseni, *Member, IEEE*

***Abstract*—A fluid dynamic algorithm based on smoothed particle hydrodynamics (SPH) is proposed for coordination of a team of unmanned aerial vehicles (UAVs) in a wireless sensor network. SPH is a Lagrangian particle method typically used to model compressible and quasi-incompressible fluid flows. In this study, SPH is used to develop a decentralized controller for a swarm of fixed-wing UAVs, which move in 3-D space under constraints of airspeed and turning radius. Vector field path-following is used to guide the swarm towards the goal. We investigate circular, racetrack and counter-rotating loiter patterns for the UAVs in the goal region. This fluid dynamics coordination treatment allows UAVs to avoid collisions with obstacles and other flying UAVs. 3-D simulations are used to test the SPH-based control algorithm. Simulations were used to explore special cases, such as the modeling of obstacles with virtual SPH particles, and the use of a variable kernel to control the inter-vehicle separation. Finally, an aerial mobile sensor network is set up using SPH as the control mechanism, and an experimental characterization of air-to-air and air-to-ground communications is conducted. The experiments use two ground stations and three Delta-wing UAVs with a wingspan of 32 inches as nodes. Each node has a IEEE 802.15.4 ZigBee radio operating in the 2.4 GHz band. The low computational costs involved in the distributed SPH-based control algorithm make it an attractive option for implementation on simple inexpensive microprocessors. The results of simulations and experiments demonstrate the viability of setting up a mobile sensor network of inexpensive UAVs based on SPH.**

***Index Terms*—Multi-agent systems, smoothed particle hydrodynamics, unmanned aerial vehicles, wireless sensor network.**

I. Introduction

UNMANNED aerial vehicles (UAVs) have shown great promise in the field of mobile sensor networking. A team of UAVs can be quickly and easily deployed in areas that are relatively inaccessible from the ground. Potential applications include diverse operations ranging from atmospheric research to reconnaissance surveillance and target acquisition (RSTA). Based on the nature of their application, UAVs vary greatly in their weight and size. Large UAVs can carry a lot of equipment on-board, and are capable of performing extremely complex tasks. However, they are heavy and pose a danger to life and property in case of a failure. Moreover, they are expensive and the cost of failure is extremely high. Small bird-sized UAVs and micro aerial vehicles (MAVs), on the other hand, are light-weight and inexpensive. They pose little or no threat to people or property on the ground and may be reused for several different applications. Most bird-sized UAVs do not require a runway or a landing strip. Owing to their low cost, several small sized UAVs may also be used to operate as a team to accomplish a given objective. A team of these vehicles can be programmed to perform various tasks based on cooperative control algorithms. Traditionally, individual UAVs have been controlled using simple potential field techniques [1], [2]. Control of UAV swarms require more sophisticated algorithms [3], or multi-layered algorithms [4], with each layer handling a specific control requirement, such as collision avoidance, trajectory tracking etc. The study of mobile sensor networks of unmanned aerial vehicles and unmanned underwater vehicles (UUVs) has been the focus area of our research group. Sensor networks consisting of UAVs are beginning to find applications in atmospheric research [3], chemical plume-detection [5], and hurricane tracking [6]. Swarms of UUVs may be used for oceanographic sensing, monitoring biological activity, and target detection [7], [8]. One of the challenges has been to incorporate a single cooperative control mechanism that would work for both UAVs and UUVs. A common approach is to use separate algorithms for the control of teams of aerial and underwater vehicles. This adds to the complexity of the combined system and doubles the effort required for development and maintenance of such systems. Controllers based on the dynamics of the fluid environment could work for both of these multi-agent systems. The difficulty is often associated with excessive cost of flow computations if the medium flow dynamics is expected to be resolved. This can be remedied by using controllers based on smoothed particle hydrodynamics (SPH).

In this paper, the control of a team of vehicles in a complex domain is treated as a fluid problem. Considering that fluid particles do not occupy the same location at the same time, and they do not penetrate into solid objects, this approach provides

Manuscript received January 15, 2010; revised July 14, 2010; accepted July 16, 2010. Date of publication September 23, 2010; date of current version January 26, 2011. This work was supported by the Office of Naval Research. The associate editor coordinating the review of this paper and approving it for publication was Dr. Robert Schober.

The authors are with the Department of Aerospace Engineering Sciences, University of Colorado, Boulder, CO 80309-0429 USA (e-mail: ashaw@colorado.edu; mohseni@colorado.edu).

Color versions of one or more of the figures in this paper are available online at http://ieeexplore.ieee.org.

Digital Object Identifier 10.1109/JSEN.2010.2064294

an intrinsic collision and obstacle avoidance algorithm. There are several other advantages to a fluid cooperation technique that are of interest to our group. Cooperation of autonomous vehicles in a heterogeneous medium (teams of aerial and underwater vehicles, for instance), can be easily accommodated in a fluid-based algorithm. In most environmental sensor networking applications, thermo-fluid information of the medium are available or calculated in parallel. As a result, this information could be easily used in a fluid cooperation algorithm. Integration of the dynamics of the medium, where the vehicles operate, into the cooperation algorithm could result in significant simplification of the overall system level complexity of the sensor network.

This paper is divided into two parts. The first part of the paper describes the theory of SPH-based cooperative control and investigates, through the use of 3-D simulations, various ways in which it could be used in the control of a team of UAVs. SPH was developed to model compressible and quasi-incompressible fluid flow which, compared to other methods, yields reasonably accurate results at lower computational costs [9]. Grid-based numerical methods like finite difference methods (FDM) and finite element methods (FEM) have traditionally been used to solve problems in hydrodynamics. FDM often uses an Eulerian grid which is fixed in space and time, and is not deformed by the flow of matter. In a Lagrangian method material elements are evolved and there is no fixed grid. Solving problems where there is a significant material deformation creates numerical challenges using fixed Eulerian grids. To this end, mesh-free Lagrangian methods, such as SPH, have significant advantages. SPH uses a set of particles to model the state of the system. The distribution of particles does not affect the formulation of SPH, and it can therefore be applied to problems involving large deformation and arbitrary distribution. SPH has found wide-ranging applications in the fields of astrophysics [10], fluid dynamics [11], and heat transfer [12]. The work of Pimenta et. al. [13] presents a SPH-based approach for controlling a swarm of robots in a 2-D pattern generation task. This theory was later extended in Pimenta et. al. [14] to include finite size and differential drive robots. Huhn and Mohseni [15] used 2-D simulations to demonstrate the use of SPH in the control of a group of UUVs with obstacle and adversarial region avoidance.

In this investigation, we apply SPH to the problem of controlling a team of UAVs, through 3-D simulations and experiments. Fixed wing UAVs are non-holonomic vehicles that move in 3-D space and are constrained to maintain a certain range of airspeed values. Additionally, these UAVs are subject to turning radius constraints. The SPH method when applied to the control of a team of UAVs provides for collision avoidance, uniform region coverage and dynamic path planning, taking into account the range and bandwidth limitations of inter-vehicle communication. The SPH method produces robust, scalable and decentralized controllers for a team of vehicles.

In this study, smoothed particle hydrodynamics is combined with vector field guidance for the control of a team of UAVs. Each vehicle is required to avoid collision with obstacles and other vehicles, and converge on a goal region. The goal region, in the case of fixed-wing aircrafts, cannot be a set of stationary points. Fixed-wing aircrafts must maintain a forward flight speed in order to remain aloft. The vehicles must, therefore, transition smoothly into a desired loiter pattern in the goal region. Circular, racetrack, and counter-rotating pair vector field patterns are computed for the goal regions. Circular loiter patterns are commonly used by UAVs in target observation, area/volume sampling, stationary loitering and waypoint navigation. Racetrack loitering has uses in convoy protection and in airstrip approach and landing maneuvers. Possible applications of the counter-rotating-circular-pair loiter patterns are obstacle avoidance and tracking of a target moving with variable speed by a team of UAVs. The vector field provides the external force that drives the team of vehicles towards the goal. The SPH treatment ensures that the vehicles have limited interaction and do not collide among themselves. The turn-radius limitations and airspeed constraints for fixed-wing aircrafts are imposed. The flight paths, velocities and accelerations for a group of vehicles are simulated in three dimensional space. The first part of the paper details and analyses the results of the simulations.

The second part of the paper details a typical application of SPH based cooperative control, which is, setting up of a mobile sensor network of UAVs. Delta-wing UAVs, with 32 inch wingspan, are used in the experiments. These UAVs are cheap and dispensable, can be produced in large numbers, and used in harsh conditions, such as hurricanes, where loss or damage to the UAVs cannot be avoided. The small size of these vehicles and their low payload capacity, impose practical constraints on the available battery power and the antenna placement. These factors are taken into account while characterizing the communications. The wireless module in each unit consists of a ZigBee radio interfaced with the microprocessor through the universal asynchronous receiver transmitter (USART). ZigBee is an industry standard for wireless networking developed by the ZigBee Alliance, formed in 2002. The ZigBee standard is based on the IEEE 802.15.4 specification for wireless personal area networks (WPANs). ZigBee is meant for applications that require a low data rate and use low power. Various industry players manufacture and sell ZigBee compliant radios. Most of them provide link quality evaluation for their radios for both indoor and outdoor environments. However, these measurements for stationary radios in indoor and outdoor environments are not necessarily valid for an airborne mobile sensor network setup. Moreover, the actual performance depends on several factors like antenna orientation, antenna height, surrounding enclosure, obstructions, etc. It is therefore advisable to conduct performance measurements with the radios installed in their final assembly. The wireless sensor network used in the experiment consisted of three Delta-wing UAVs, controlled by the SPH based algorithm, and two ground station units. Tests were conducted to characterize air-to-air and air-to-ground communications. Received signal strength indicator (RSSI) and packet error rate (PER) were used as the performance metrics.

This paper consists of two major sections: Section II summarizes the theory of smoothed particle hydrodynamics. We then perform 3-D simulations of different scenarios, illustrating the capabilities of the SPH based cooperative controller. We also investigate circular, racetrack and counter-rotating loiter patterns

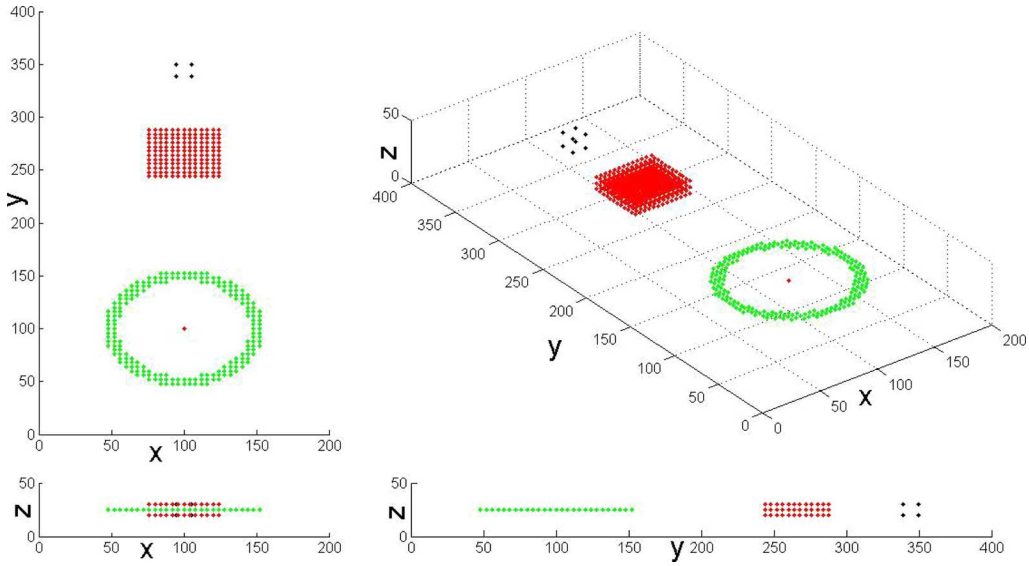

Fig. 1. World geometry in 3-D space showing a team of vehicles in their starting position, an obstacle in the center and the goal region in the form of a loiter circle.

for the UAVs in the goal region. In Section III we study a real world cooperative control application, in which an aerial wireless sensor network is set up using SPH as the underlying control algorithm. The experiment characterizes the air-to-ground and air-to-air wireless links, and the results are presented.

II. 3D Simulation of a System of Fluid Controlled Vehicles

A. Vector Path Following

For certain applications, it may be required to ensure that a particular UAV is at a particular position in a given time. Such applications require a stringent trajectory tracking control mechanism [4]. Trajectory tracking for light-weight slow-moving UAVs is difficult under gusty wind conditions. Moreover, such a high level of control is not required for most applications, including the setup of a wireless sensor network of UAVs for atmospheric sampling. The alternative is to use a path following approach [16], which is less constrained in nature. Path following focuses on guiding the vehicle towards the path, and maintaining a desired speed along the path. Vector field path following method allows for such an approach, and is sufficient for applications such as perimeter surveillance, air traffic holding patterns, area /volume sampling, and target search.

For the simulations, we generate a vector field for a world geometry in three dimensional space consisting of an external region with an obstacle, and a goal region, as shown in Fig. 1. The vector field is divided into a goal region and an external region. This is similar to the belt zone technique used in [17]. The external region is derived by solving Laplace's equation and using the goal, world boundaries and obstacles as boundary conditions. The goal region is obtained by superposing circulation components on the vector field in the vicinity of the goal. Note that the governing equations for the creation of the vector fields are linear and, as a result, superposition can be easily employed to generate more complex vector fields. The following sections describe the generation of the vector field for both the regions.

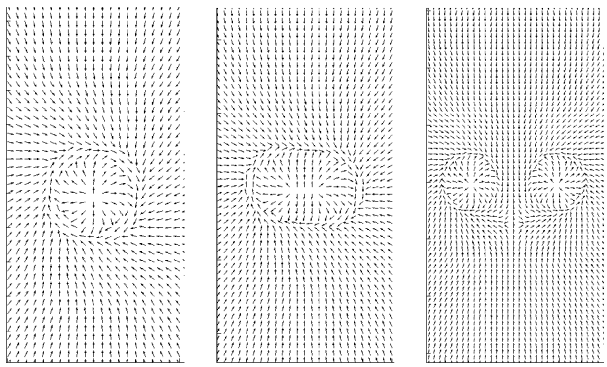

(a) (b) (c)

Fig. 2. Vector field in the goal region with (a) circular, (b) racetrack, and (c) counter-rotating loiter patterns.

1) External Region Vector Field Generation: The vector field for the external region is generated using a harmonic function which is computed by solving

$$\nabla^2 \phi = 0. \tag{1}$$

The finite difference method (FDM) was employed to solve for the potential field using a maximum value equal to one at the outer boundaries and the obstacle, and a minimum value equal to zero for the goal. The gradient of the potential field results in the desired vector field for the external region.

2) Goal Region Vector Field Generation: Different goal geometries were created by using a suitable circulation function in the goal region. A circulation component, given by (2), was superposed to allow the vehicles to transition smoothly into a circular loiter pattern, on reaching the goal region

$$\phi_{rot} = \begin{cases} \frac{a}{R} r(-\sin\theta \widehat{e}_x + \cos\theta \widehat{e}_y) & 0 < r < R \\ \left(\frac{2a}{r} - \frac{a}{R}\right) r(-\sin\theta \widehat{e}_x + \cos\theta \widehat{e}_y) & R < r < 2R \end{cases} \tag{2}$$

where r is the distance from the center of the goal, θ is the angle from the positive x-axis, a is the circulation strength and R is the radius of the goal. The circular, racetrack and counter-rotating loiter patterns obtained for the simulation are shown in Fig. 2.

These loiter patterns in the goal region ensure that the UAVs continue to maintain a desirable airspeed on reaching the goal.

B. Smoothed Particle Hydrodynamics

We treat the control of the swarm of vehicles as a fluid flow problem, where each vehicle is treated as a particle in an incompressible fluid. SPH can be used to model incompressible fluids by choosing low Mach number values [9]. The use of SPH provides a computationally tractable method to control a large number of UAVs/UUVs in a decentralized way. At the same time, this treatment allows the entire swarm to be viewed as a freely flowing incompressible fluid with known predictable behavior.

1) Interpolation Kernel: The SPH method converts the governing continuum equations of fluid dynamics to a set of ordinary differential equations. A differentiable interpolation kernel, which approximates a delta function, is used to perform this conversion. There are several forms that this kernel can take, so long as they satisfy a set of conditions described by Li and Liu [18]. Commonly used kernels are the Gaussian function, the quadratic spline function and the cubic spline function. In this study, we choose the cubic spline kernel for the SPH calculation. This kernel has a smoothing length, h, which defines a region that confines the major part of the kernel function. This provides for computational efficiency since only the particles in a certain region have to be considered in the summations. For our purpose, this choice of kernel is preferred over, say, a Gaussian kernel, in which every particle must be included in the SPH calculation, even though the contribution from distant particles is negligible. Moreover, when applied to the control of a group of vehicles, the smoothing length of the cubic spline kernel provides for restricted interaction between the vehicles. This is achieved by choosing a kernel with a smoothing length h that takes into account the contributions of only those vehicles that are within the range of communication. The cubic spline interpolation kernel utilized for this paper is given by

$$W(r,h) = \frac{10}{7\pi h^2}\begin{cases} 1-\frac{3}{2}s^2+\frac{3}{4}s^3 & \text{if } 0 \le s \le 1 \\ \frac{1}{4}(2-s)^3 & \text{if } 1 < s \le 2 \\ 0 & \text{if } 2 < s \end{cases} \tag{3}$$

where $s = \|r\|/h$, r is the distance between the two particles, and h is the smoothing length of the kernel. The choice of the interpolation kernel described in (3) ensures that the contribution of any vehicle more than $2h$ away is neglected. The plots of the cubic spline kernel for three different values of h are presented in Fig. 3.

2) Artificial Viscosity: Utilizing the interpolation kernel to transform the classical fluid conservation equations, the SPH conservation equations for density, momentum and energy of a single particle are obtained in the form given by [9]

$$\begin{aligned} \rho_i &= \sum m_j W(r_{ij},h) \\ \frac{dv_i}{dt} &= -\sum m_j\left(\frac{P_i}{\rho_i^2}+\frac{P_j}{\rho_j^2}+\Pi_{ij}\right)\nabla_i W(r_{ij},h)+G_i \\ \frac{de_i}{dt} &= \frac{1}{2}\sum m_j\left(\frac{P_i}{\rho_i^2}+\frac{P_j}{\rho_j^2}+\Pi_{ij}\right)v_{ij}\cdot\nabla_i W(r_{ij},h) \end{aligned} \tag{4}$$

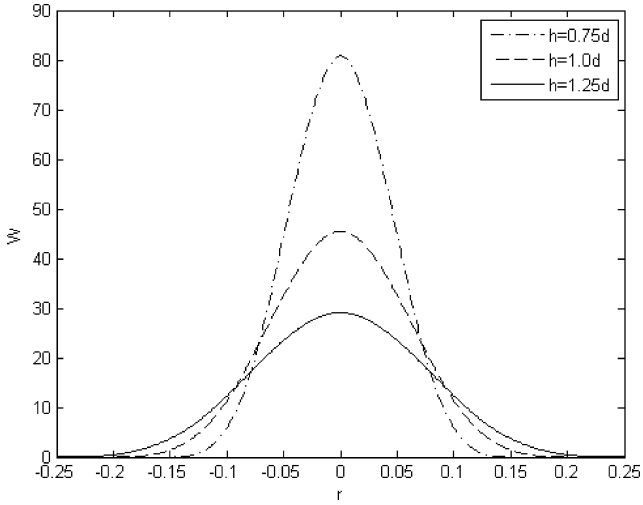

Fig. 3. Cubic spline kernel for different values of smoothing length.

where v is velocity, e is energy, P is pressure, r_i is the position vector of particle i, ρ is density, ∇_i is the gradient with respect to the position of particle i, G_i is the sum of the external forces normalized by mass m, $r_{ij} = r_i - r_j$, $v_{ij} = v_i - v_j$ and Π_{ij} is the artificial viscosity. The artificial viscosity term used here is the same as the one suggested by Monaghan [9], given by

$$\Pi_{ij} = \begin{cases} \frac{1}{\overline{\rho}_{ij}}(-\alpha\overline{c}_{ij}\mu_{ij}+\beta\mu_{ij}^2) & \text{if } v_{ij}\cdot r_{ij} < 0 \\ 0 & \text{if } v_{ij}\cdot r_{ij} \ge 0 \end{cases} \tag{5}$$

where

$$\mu_{ij} = \frac{h v_{ij}\cdot r_{ij}}{\|r_{ij}\|^2+\eta^2} \tag{6}$$

where α and β are positive constants, $\overline{\rho}_{ij}$ and $\overline{c}_{ij}$ are the average density and speed of sound of i and j, respectively and η is a constant to avoid singularities and should be small ($\eta = 0.1h$) to prevent extreme smoothing of the viscous term in high density regions. Choosing this value for η allows smoothing of the velocity to occur only if the spacing is less than $0.1h$. Note that the viscosity term vanishes when $v_{ij}\cdot r_{ij} > 0$, which is the SPH equivalent of the condition $\nabla\cdot v > 0$.

3) Quasi-Incompressible Flow: Using SPH for the control of a team of UAVs requires the flow to be modeled as being incompressible. SPH was designed for compressible flow problems, but it can be extended to nearly incompressible flow [9]. Compressibility effects can be brought down by choosing a very small Mach number, M, in an artificial equation of state given by

$$P_i = B_i\left[\left(\frac{\rho_i}{\rho_o}\right)^{\gamma}-1\right] \tag{7}$$

where ρ_o is the reference density, γ is the specific heat ratio, and B_i is the bulk modulus. The bulk modulus is computed using

$$B_i = \left(\frac{\|v\|_{\max}}{M}\right)^2\rho_i. \tag{8}$$

The bulk modulus is a ratio of the maximum velocity of the flow and the Mach number, M. In order for the fluid to be modeled as nearly incompressible the Mach number needs to be small (0.1 – 0.01), since the compressibility effects are $O(M^2)$. By choosing

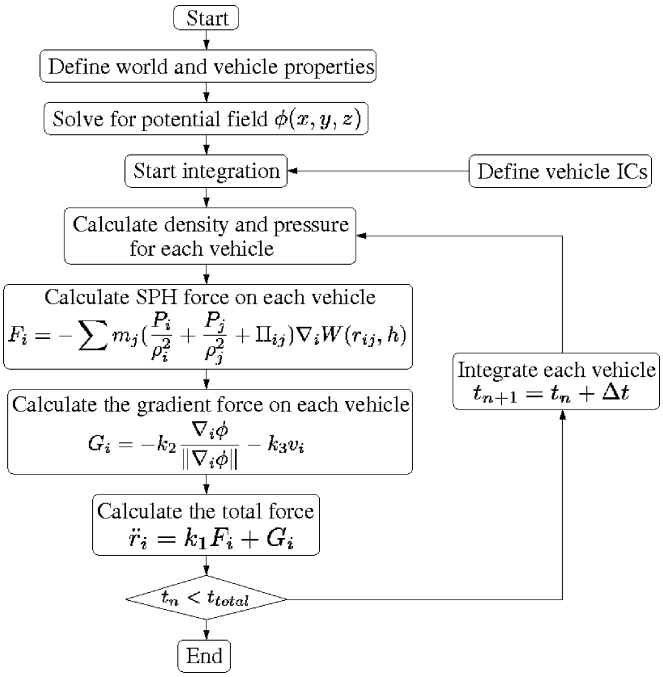

Fig. 4. Flow diagram for the SPH simulation for a swarm of UAVs.

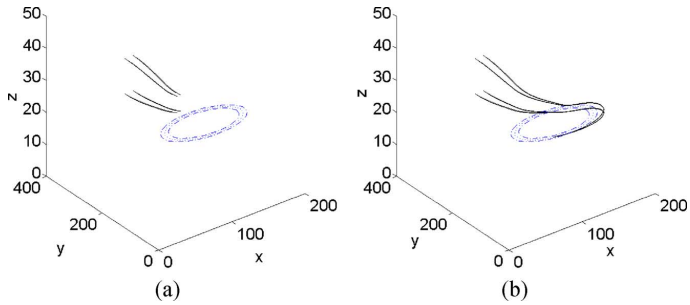

Fig. 5. Path lines for flow of vehicles from different altitudes into clockwise circular loiter pattern at (a) time t = 30 s and (b) t = 50 s.

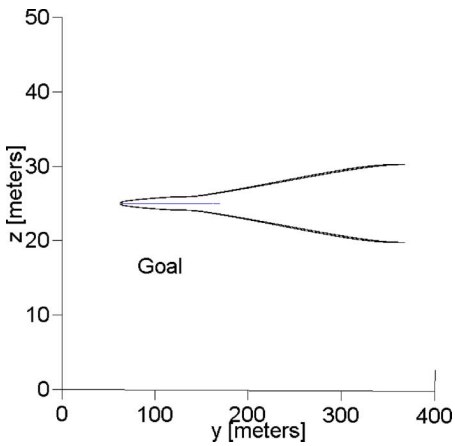

Fig. 6. Path lines for vehicles as they adjust their altitudes to enter the loiter circle. This is a view of the path lines, showing the y-z axis. The circular goal when viewed from this perspective appears as a line segment at z = 25.

ρ_o, the reference density to be equal to that of water, and by using a low Mach number, the flow of the UAVs is modeled to be very similar to the flow of a liquid; in this case, water.

C. Control Law

Internal forces due to SPH and external forces due to the vector field propel the vehicles along their paths toward their goal. We use a control law for the UAVs which is the same as the one used by Pimenta et. al. [13] for the control of a swarm of ground robots. The control law for a vehicle, i, is given by

$$\ddot{r}_i = k_1 F_i + G_i \tag{9}$$

where

$$F_i = -\sum m_j \left(\frac{P_i}{\rho_i^2} + \frac{P_j}{\rho_j^2} + \Pi_{ij} \right) \nabla_i W(r_{ij}, h) \tag{10}$$

$$G_i = -k_2 \frac{\nabla_i \phi}{\|\nabla_i \phi\|} - k_3 v_i \tag{11}$$

where k_1, k_2 and k_3 are constants, F_i represents the inter-vehicle forces due to SPH, and G_i is the external force acting on each vehicle due to the vector field. P_i and P_j represent the hydrostatic pressure computed using (7) for particles i and j respectively.

D. Simulation

In order to analyze the dynamics of this control algorithm, simulations were created in the MATLAB environment. A flow diagram of the simulation is presented in Fig. 4. A typical simulation run starts with a given number of vehicles arranged in the form of a three dimensional grid as shown in Fig. 1. Fig. 5 shows the path lines of the vehicles as they converge towards the goal (Fig. 5(a)), and begin to loiter at the appropriate altitude (Fig. 5(b)). The top layer of the grid typically consists of vehicles that have been placed at an elevation higher than that of the goal region. The bottom layer has vehicles that are at a lower altitude compared to the goal region. This forces the vehicles to adjust their altitude during their flight towards the goal as shown in Fig. 6. In this case, the circular goal is at an altitude of 25 meters, and the vehicles are distributed in two planes, one at an altitude of 20 meters and another at an altitude of 30 meters. The path lines highlight how the vehicles gradually converge to the correct altitude. The SPH based control law ensures that the vehicles maintain safe distance from each other and avoid obstacles along their path to the goal. Moreover, SPH forces in the control equation also ensure that the vehicles loitering in the goal region are always separated by a fixed distance equal to twice the smoothing length. This can be used to get the UAVs into interesting geometric formations during flight.

It is to be noted that each vehicle is required to compute its own density and hydrostatic pressure, and transmit this information to other vehicles within its communication range. This simplifies the computation to be performed on-board each vehicle. The fact that the smoothing length intrinsically accounts for the range limitation of inter-vehicle communication permits the use of simple single-hop broadcast systems operating at low power.

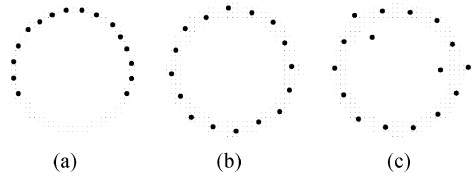

Fig. 7. Distribution of vehicles in a circular pattern for various values of h/d (a) 1.5, (b) 2.5, and (c) 3.0.

1) Calculation of the Smoothing Length: This simulation was performed with various values of the smoothing length h, which is bounded by the range of communication of the vehicles. Any vehicle outside of the communication range of $R = 2h$ will not be able to contribute to the SPH dynamics for that vehicle. The smoothing length controls the inter-vehicle spacing. In the external region, the inter-vehicle spacing is required only to prevent collisions between the vehicles. In the goal region, however, the smoothing length is used to control the distribution of vehicles. Fig. 7 shows the distribution of 16 vehicles in a circular loiter pattern, of radius 50 meters, for various values of the smoothing length h non-dimensionalized by the grid spacing d, which has the value of 4 meters in the simulation. From these results, it is evident that if the h value is too low (Fig. 7(a)), then the vehicles will bunch at the goal and not distribute evenly. On the contrary, if the h value is too high (Fig. 7(c)) then the vehicles will disperse better but will cause crowding and force some vehicles out of the nominal goal centerline. Therefore, the value for h needs to be chosen properly for the number of vehicles and the geometry of the goal. From Fig. 7, it seems that h/d of approximately 2.5 is an appropriate choice for the simulation presented. The radius of the goal circle is $12.5d$; therefore the closed curve that the vehicles are required to converge on is approximately $78.54d$. In order for the 16 vehicles to distribute evenly the spacing should be $4.909d$, which is approximately twice the h value simulated for convergence. It may be seen that in order to evenly pack in a large number of vehicles into a given pattern, the following relation should be satisfied

$$h = \frac{l}{2N_v} \tag{12}$$

where N_v is the number of vehicles and l is the perimeter of the closed curve of the goal. This generalized equation works for all three types of loiter patterns presented here.

2) Calculation of the Control Gains: The magnitude of the SPH force, F_i, and the gradient force, G_i, acting on the vehicle i is modulated by the value of the gains k_1, k_2 and k_3. The SPH force sets in when vehicles get too close to each other. The gradient force drives the vehicle towards the goal. The magnitude of the gradient force must be suitably balanced in order for the vehicle to maintain a desired airspeed. From (11), it can be seen that in order to maintain an airspeed v, the gains k_2 and k_3 must satisfy the condition given by (13)

$$v = \left\| \frac{k_2}{k_3} \right\|. \tag{13}$$

The value for the gain k_1 is estimated such that the force due to SPH is of the same order of magnitude as the external force F_i.

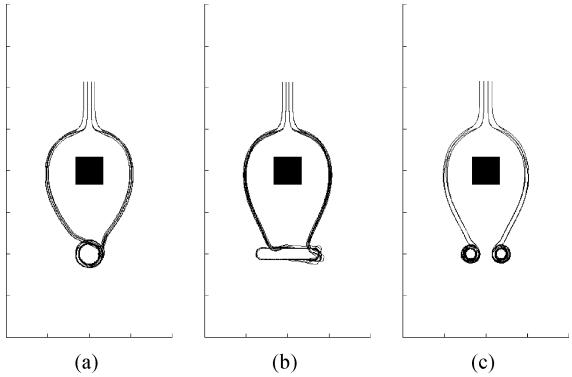

Fig. 8. Path lines for flow of vehicles around an obstacle into (a) clockwise circular, (b) racetrack, and (c) counter-rotating loiter patterns.

E. Simulation Results

Utilizing the various vector fields that we discussed earlier, simulations were conducted to verify if the vehicles will converge on the goal regions and circulate in the desired shapes. The path lines for an arbitrary circle, racetrack and counter-rotating pair are presented in Fig. 8. After determining that these circulation patterns were possible using our SPH controller, each of these goal types was investigated further to characterize their limitations. First, a simulation was conducted in search of how to force the vehicles to converge upon a circular goal and distribute evenly as they circulate about it. An eighty second simulation was performed and the motion of the vehicles is presented in Fig. 9. The vehicles avoid the obstacle and are guided towards the circular loiter goal region. Fig. 9(e)–(i) focuses on the sequence of vehicle movements when they arrive at the goal region. The SPH controls the inter-vehicle spacing and determines how the vehicles are distributed in the goal region. After the vehicles enter the circle in two distinct groups, some of the vehicles are initially placed on the nominal goal line and others are on the outside trying to procure a space in the goal. As time progresses, vehicles are able to squeeze into the nominal configuration. At the end of the simulation all of the vehicles have secured a place in the goal and are rotating with a near constant velocity. The case that is studied in this run is same as the h/d value that is prescribed in (12) for the case with no circulation. Therefore, it seems that the circulation has no effect on the value of h/d necessary for the vehicles to converge on the goal, assuming that the velocities are able to fluctuate to allow merging of vehicles into the formation. During the initial part of the simulation, where the vehicles move around the obstacle and towards the goal, the external force due to the vector field dominates. The role of the repulsive inter-particle forces due to SPH becomes more significant when the particles arrive at the goal region. This is demonstrated in Fig. 10, where the magnitude of the two forces F_i, due to SPH and G_i, due to the vector field, in the direction of motion of one vehicle are presented. It is to be noted that the forces have been resolved in the direction of motion, and are, therefore, indicative of the changes in speed of the vehicle. It is evident that the forces due to SPH spike when the vehicles enter the loiter circle at approximately $\mathrm{t} = 30\,\mathrm{s}$ and settle as the spacing becomes adequate. The gradient force, resolved along the direction of motion, is zero for most part of the simulation, indicating that it acts to guide the vehicles without accelerating them.

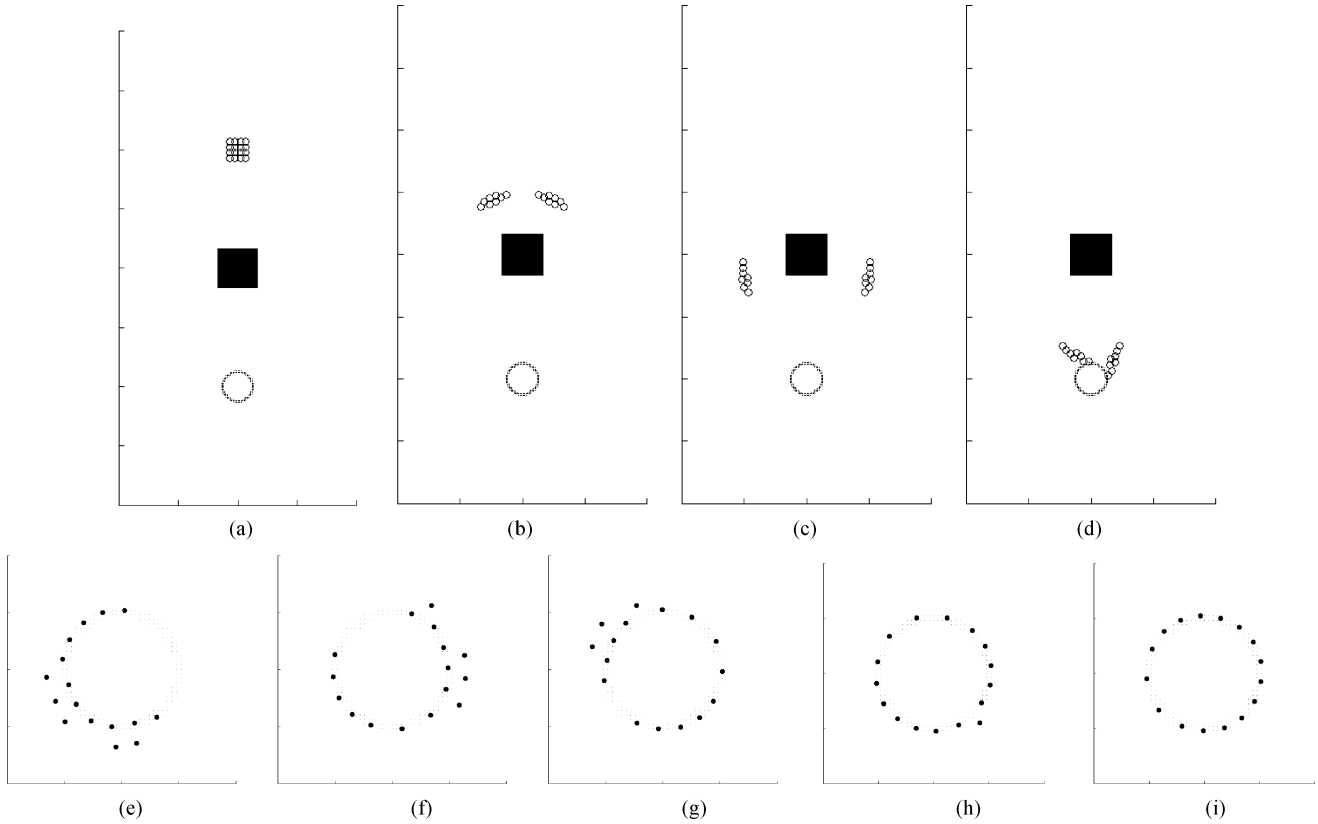

Fig. 9. Simulation results of sixteen vehicles for a circular loiter goal with $h/d = 2.5$. (a)-(d) show the movement of vehicles in the external region consisting of an obstacle for the first 30 seconds of the simulation time. (e)-(i) show how the vehicles settle into the circular loiter pattern. (a) $\mathrm{t} = 0$. (b) $\mathrm{t} = 10$. (c) $\mathrm{t} = 20$. (d) $\mathrm{t} = 30$. (e) $\mathrm{t} = 40$. (f) $\mathrm{t} = 50$. (g) $\mathrm{t} = 60$. (h) $\mathrm{t} = 70$. (i) $\mathrm{t} = 80$.

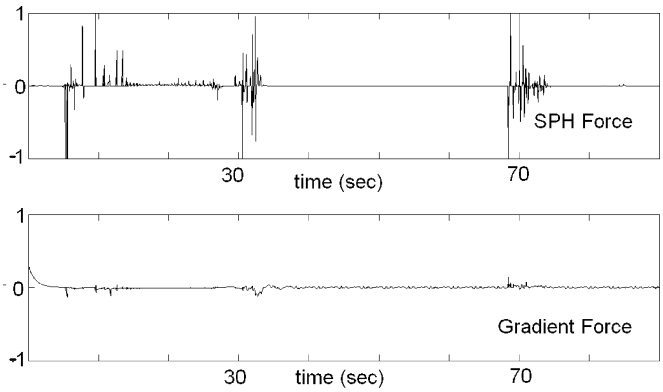

Fig. 10. The magnitudes of normalized SPH and gradient forces acting on a vehicle.

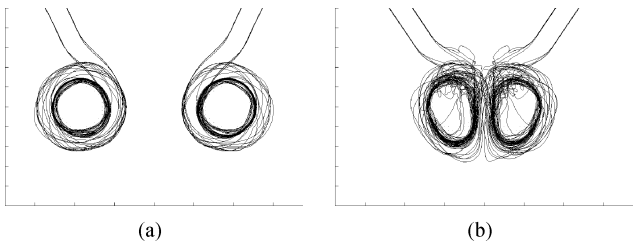

Fig. 11. Counter-rotating loiter pattern with 16 vehicles with a loiter circle spacing of (a) 0.75 and (b) 0.3.

In addition to the circular goal case, an attempt was made to characterize the counter-rotating loiter circle pair and determine what variables affect the convergence of the fleet into two equally spaced subgroups. Assuming that (12) holds true for this case, the major variable of concern is the spacing of the two loiter circles. In Fig. 11, the cases of placing these loiter circles sufficiently far apart and too close together are examined. In the case where the loiter circles are sufficiently spaced, as in Fig. 11(a), the group divides in two and behaves as two independent single circle scenarios. As the spacing between the loiter circles is decreased the loiter circles appear to deform, as may be seen in Fig. 11(b). Even though the path is deformed from the nominal goal prescribed, it seems that the distribution of the vehicles is divided evenly between the two circles.

Finally, the case of a racetrack loiter pattern was considered and the path lines for sixteen vehicles in the goal area is presented in Fig. 12. A less than nominal h/d value was utilized and the vehicles manage to move around the nominal racetrack centerline. There is a minor amount of movement away from the track when the vehicles move around the circular portions of the course. It was seen, that setting a small value of the circulation strength, a, in the (2), minimizes the end-effects of the racetrack pattern. Moreover, in Fig. 12, it is important to note the erratic motion as the vehicles enter the goal region. Both subgroups of the flock enter the track at approximately the same time, however, because the circulation strength is not strong enough, the vehicles do not smoothly transfer into this loiter pattern. Studies into the effects of circulation strength, a, were performed and

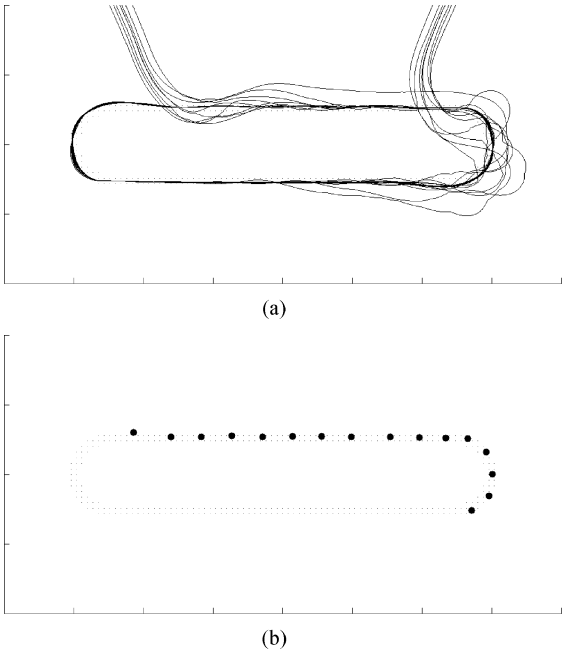

Fig. 12. Racetrack loiter pattern with 16 vehicles showing (a) path lines and (b) vehicle distribution for lower than nominal h/d value.

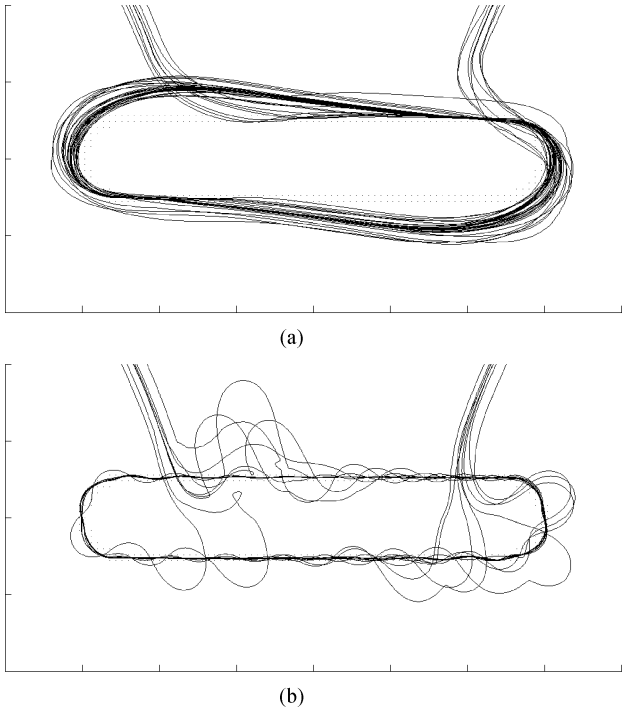

Fig. 13. Racetrack loiter attractor path lines for 16 vehicles with circulation strengths of (a) $a = .0625$ and (b) $a = .0039$.

the results for two different strengths are presented in Fig. 13. It is evident that as the circulation strength is decreased, the vehicles stay on the centerline of the racetrack better, and the distortion at the semicircular ends of the racetracks are minimized. However, with a lower circulation strength, it is also noticeable that the transitions into the racetrack loiter is not as smooth. A composite controller is proposed such that the benefits of a

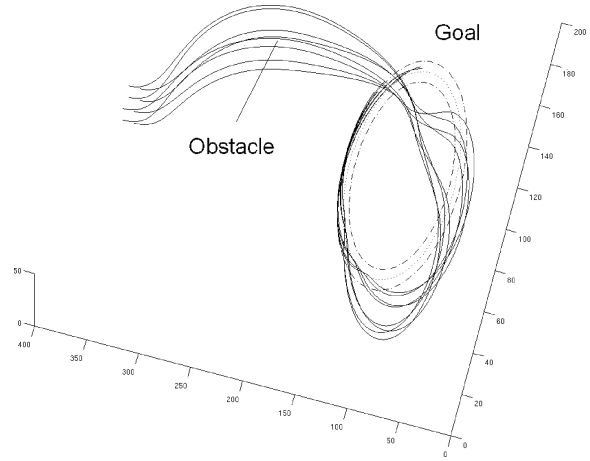

Fig. 14. Path lines of vehicles in 3-D space, showing their flow over a wall-like obstacle modeled by virtual SPH particles.

smooth transition into the racetrack and maintaining a tighter racetrack loiter pattern are achieved.

1) Adaptive Path Planning Using Virtual SPH Particles: In some applications, we may need to specify an adversarial region which the vehicles are required to avoid. In other cases, vehicles may be equipped with short range sensors (optic flow sensors, for instance) to detect obstacles in their path. Discovery of such obstacles during flight requires an immediate change in the flight path. As SPH particles exert repulsive forces on particles in their neighborhood, it is possible to model obstacles or adversarial regions with one or more virtual SPH particles. A row of such virtual particles may be used to represent a wall-like obstacle. 3-D simulation runs with such a wall modeled using virtual SPH particles forced the vehicles to change their path. The vehicles were seen to avoid the wall by moving over it. Fig. 14 shows one such simulation run in which a swarm of vehicles move from the left, towards the goal in the right, flowing over the wall-like obstacle. The fact that stationary SPH particles can model obstacles allow for dynamic path planning for vehicles. Whenever a vehicle senses an obstacle in its path, it can model it as a virtual SPH particle. This will cause the vehicle to adapt to its immediate surroundings, avoid adversarial regions and obstacles using the same SPH mechanism at little extra computational cost. It should be noted that the virtual particles need not be stationary. In more complex applications, these particles may also be used to model moving obstacles.

2) Adaptive Coverage Optimization Using Variable Smoothing Length: The smoothing length h controls the inter-vehicle separation. In the external region of the simulated world geometry, the value of the smoothing length should be chosen to prevent collision between the vehicles as they travel. However, in the goal region, the value of the smoothing length should be chosen for the uniform distribution of the vehicles. The smoothing length, h, in the goal region should, therefore, be different from the value of h when the vehicles move towards the goal. In order to achieve this behavior, a spatially-varying smoothing length is used in the simulation. The smoothing length of the vehicles is changed as they enter the goal region. The vehicles are able to enter the goal region more tightly packed and then expand to an equal distribution,

resulting in better performance. In some applications, a temporally-varying smoothing length may be used, in which the value of the smoothing length is globally changed at a given time.

Changing the smoothing length also allows for readjustment of inter-vehicle separation in the goal region in case of failure of one or more units. If a swarm of UAVs lose a few units on the way to the goal region, the value of h can be recalculated using (12). This would allow for uniform coverage in the goal region regardless of the number of vehicles. This technique is limited in its application by the fact that it requires a centralized control mechanism to keep track of the number of functioning units. However, if the maximum inter-vehicle separation in the goal region is smaller than the communication range, it would be possible for each vehicle, in the goal region, to adaptively change its value of h based on the number of vehicles it is able to communicate with. Alternatively, a decentralized mechanism for adaptive coverage optimization may be devised using the fact that in the types of goal regions described earlier, any given vehicle interacts with exactly two neighboring vehicles in an optimal arrangement. In Fig. 12, the vehicles are not distributed uniformly in the racetrack loiter pattern, as the value of the smoothing length h is lower than nominal. However, as the vehicles settle to their steady state velocities, the SPH forces of interaction between the vehicles is limited to its immediate neighbors. Every vehicle, other than the two vehicles at the extremities, interact with exactly two other vehicles. This information may be used by the network, to adaptively tune the inter-vehicle spacing to approach optimal coverage. The vehicles that sense fewer than two neighbors, will respond by increasing their smoothing length in small increments. Additionally, they will transmit the new value of the smoothing length, h, to their neighbors, causing them to adjust their values of h, until the system converges to a optimal coverage distribution. A SPH controlled wireless sensor network, set up in this manner, is decentralized and has self organizing capabilities. Moreover, in a single-hop wireless sensor network, each node can receive data from only those nodes that are within its communication range. In a SPH-based controller, this limitation imposed by the communication range is inherently accounted for by means of the smoothing length. The SPH-based controller does not require information about any node that lies outside the smoothing length, and therefore, exhibits no degradation in performance due to range limitations.

III. Wireless Communication Characterization

Having developed a theoretical foundation for SPH based cooperation backed by 3-D simulations for various scenarios, we deployed it in a simple wireless sensor network consisting of two ground stations and three aerial vehicles. We, then, used this SPH driven wireless sensor network, to characterize the IEEE 802.15.4 ZigBee based wireless communications. A number of previous work [19]–[21] focus on characterizing 802.15.4 radios at 2.4 GHz in stationary indoor and outdoor environment. However, it is for the first time that performance measurements are being conducted on the 802.15.4, 2.4 GHz ZigBee radios on a *mobile* network using aerial vehicles of *this* scale. The data collected from the experiment is also valuable in determining the bounds on some SPH parameters. The subsequent sections will focus on describing the wireless characterization experiment and its results.

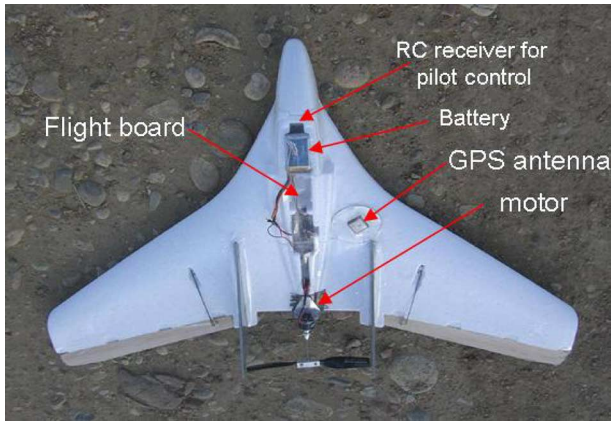

Fig. 15. A 32-inch Delta-wing UAV used in the experiment.

Fig. 16. CUPIC autopilot weighs 19 grams and is 6 cm × 3 cm × 1.4 cm in dimensions.

A. Hardware Configuration

1) The Delta-Wing UAV: The Delta-wing aircraft shown in Fig. 15 weighs less than 0.5 kg and has a wing span of 0.8 m. The design of these vehicles is relatively simple and it is easy to produce them in large numbers, and equip them with an autopilot for fully autonomous operation, including take-off and landing. Thus, these Delta-wing UAVs are highly suited for wireless communication characterization tests using the SPH based control system. The distributed logic for the SPH-based control was implemented on the microprocessor on the CUPIC.

2) The Cupic Autopilot: The CUPIC, shown in Fig. 16 is an autopilot system developed entirely in the University of Colorado at Boulder [22]. Several studies [2], [5] have shown that it is possible to achieve fully autonomous operation of a small UAV by means of a simple autopilot equipped with a limited number of sensors. The CUPIC, in its most basic design, consists of an on-board processor, a single axis rate gyro to sense roll rates, an absolute pressure sensor for altitude sensing, and a GPS receiver for positioning. The board includes the Digi XBee PRO radio and Fastrax Itrax 03–02 GPS, and detachable ADXRS150EB single axis rate gyros. The CPU used in the CUPIC autopilot is Microchip's PIC18LF8722. The on-board program is written in the C programming language. This program outputs commands to the motor and servos via the on-board PWM interface. The program has built-in routines to account for short term blackouts in the GPS signals and the

TABLE I
WIRELESS SETUP

Wireless Module	Digi XBee Pro
MAC and PHY Protocol	IEEE 802.15.4
Frequency	2.4 GHz
Transmit Power	10mW
Data Rate	57600 baud
Packet Size	64 bytes
Transmission Frequency	100 Hz

noise and drifts in the sensors. The autopilot has been proven to be fully capable of stable autonomous flight on a wide variety of MAVs including Delta-wing aircrafts [5], Warping-wing aircrafts, and Gust-insensitive aircrafts [23].

3) The Ground Station: The Ground station allows the transmission of commands to the CUPIC and the reception of telemetered data from the CUPIC. The ground station consists of an XB Pro Radio Unit and a graphical user interface to view the telemetered data real-time. The graphical user interface includes launch and land command options, and options to change the loiter center co-ordinates and radius of each UAV separately. The ground station, in its current version, supports the control of five aircrafts simultaneously.

4) Wireless Setup: The wireless setup consists of IEEE 802.15.4 compliant Digi's XBee Pro radios operating in the 2.4 GHz band. Digi's XBee Pro radios conform to the ZigBee standards and are small, light-weight and easily interfaced with the PIC processor via a serial interface. The transmission is set to broadcast mode. Air-to-air links are set up between the UAVs and air-to-ground links are setup between the UAVs and the ground stations. The radios on the UAVs transmit and receive packets to and from all UAVs in range. The ground stations simply receive packets from the UAVs and do not transmit any packets. Acknowledgments and retransmissions are disabled in order to measure packet error rates. The transmit power is set to the lowest level of 10 mW. The data rate is set to 57600 baud and the software transmits packets at 100 Hz. The size of each packet is 64 bytes. Multi-hop routing was disabled for the wireless setup. The details of the wireless parameters are summarized in Table I. The UAVs are commanded to move in circles of radius varying from 50 meters to 100 meters, at an altitude of about 50 meters from the ground. Two ground stations are positioned on either side of the loiter area of the UAVs in such a way that the UAVs are always within transmission range of at least one ground station. This set up ensures that position data from all the UAVs is available at all times during the experiment. This provides an accurate measure of packet loss in relation to the distance between a UAV and a ground station.

B. Experimental Results

Experiments were conducted on open grounds with few trees and electric poles on the ground. The ground station was set up on the ground with no trees within 100 meters of the antenna. The ground station radio did not transmit any packets; it simply received packets from the UAV radios. The UAVs performed

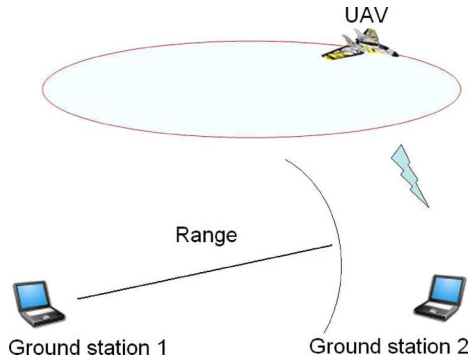

Fig. 17. Two-receiver setup ensures that the UAV is always within communication range of at least one ground station.

loiter circles of radius 100 meters at an altitude of about 30 meters from the ground. The two ground stations were positioned 400 meters apart. The three Delta-wing UAVs were uniformly distributed in the circular loiter pattern, the center of which was gradually shifted from one ground station to the other. The UAV radios transmitted packets to the ground station and other UAVs in broadcast mode. The UAV radios also received packets from other UAVs. A simple checksum was used to determine if a received packet was valid. Invalid packets were discarded and no retransmissions were attempted. The packets used in the communication were given sequential packet numbers and the gaps between the packet numbers were used to determine the number of packets being dropped in the RF link. Packet error rate (PER) and received signal strength indicator (RSSI) were used as performance metrics. It must be noted that RSSI values are not available for dropped or invalid packets. Thus, the RSSI is not very useful in the outer fringes of the communication range with high PER. Taken together, the RSSI and the PER measurements provide the required characterization for the communication links. Another communication consideration for the application is the packet gap size. Packet gap size is the total number of consecutive packets that were dropped in the transmission. Though the application has some level of tolerance for dropped packets, large sized gaps can adversely affect the functioning of distributed algorithms which depend on the data received from other nodes. Thus, it is important to characterize how the packet gap size varies with distance. The scatter plot for the packet gap size versus distance from the ground station is shown in Fig. 18. The plot shows a marked increase in the packet gap size as the distance from the ground station increases. However, at the edge of the communication range, about 200 meters in this case, the packet gap size seems to drop off to low values. This portion of the data is misleading, as very few packets get successfully transmitted beyond the communication range. A bulk of these dropped packets get assigned to the distance values just prior to the range. It should be understood that neither RSSI nor packet gap size may be used to characterize the communication at the outer limits of the communication range.

A range test was conducted for the air-to-ground links. The received signal strength indicator provided by the XBee RF Modules measures the signal strength in dB. The XBee radios were found to receive data correctly up to an RSSI of about -80 dB, but at lower RSSI values, the packet errors increased

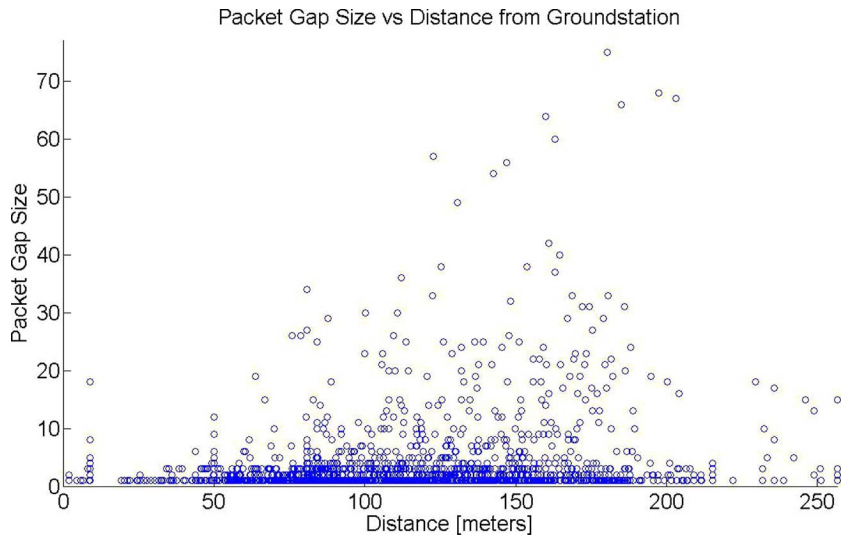

Fig. 18. Packet drop gap size versus distance from the ground station.

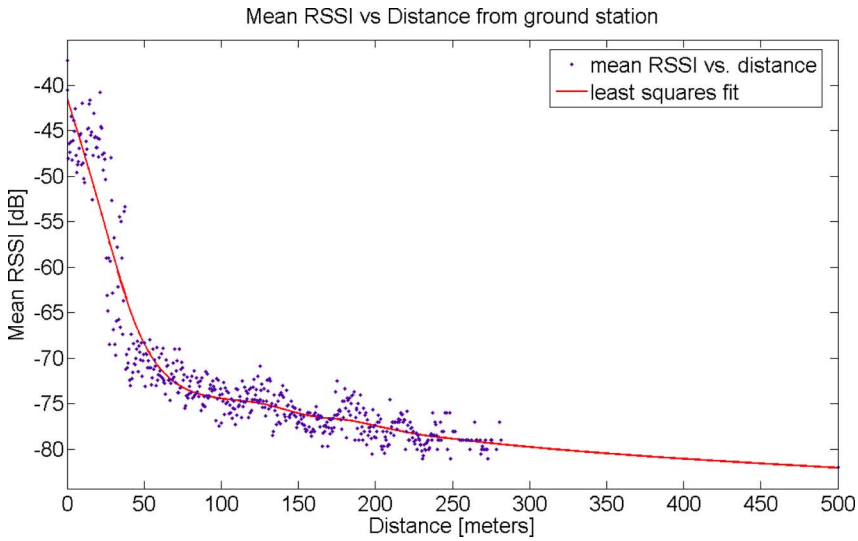

Fig. 19. Received signal strength (air-to-ground) versus distance from the ground station.

significantly. It should be noted that RSSI data was not recorded for packets that failed the checksum test. Thus, the RSSI data has no information about the packets that were invalid or dropped. The scatter plot of the mean RSSI in dB versus the distance from the ground station is shown in Fig. 19. From the plot, it is seen that RSSI values are not available for air-to-ground links beyond a distance of 200 meters from the ground station. This indicates that the effective range of air-to-ground communication is 200 meters. The values range from a maximum of -45 dB at the vicinity of the ground station, to about -75 dB near the limit of the communication range. A similar range test was conducted for air-to-air RF links. The scatter plots of the received signal strength in dB versus the separation between the aerial vehicles is shown in Fig. 20. Though the transmit power of the nodes is the same, the air-to-air links seem to perform better than the air-to-ground links. The RSSI for air-to-air drops off with the distance of separation, in a manner similar to the air-to-ground links, but at a slightly reduced rate. Moreover, the RSSI values for air-to-air links are available through a greater range of distance. In the case of air-to-ground links, the RSSI values are largely absent beyond 200 meters, whereas in the air-to-air links, valid data packets are received up to a distance of 500 meters.

RSSI may be used for estimation of inter-node distances using a log-normal radio propagation model [24]. The path loss exponent (PLE), a key parameter in the log-normal model, is obtained from the slope of the linear regression of RSSI on distance in the logarithmic scale, using

$$Pd_{ij} = -10n\log(d_{ij}) + Pd_0 \tag{14}$$

where Pd_{ij} is the RSSI in dB measured for the communication link from node i to node j, n is the path loss exponent, d_{ij} is the distance between the nodes i and j, and Pd_0 is the y-intercept of the linear fit. The plot of RSSI versus log of distance of separation for air-to-air links is shown in Fig. 21. The value of the PLE, n calculated from this plot for air-to-air links is 0.93.

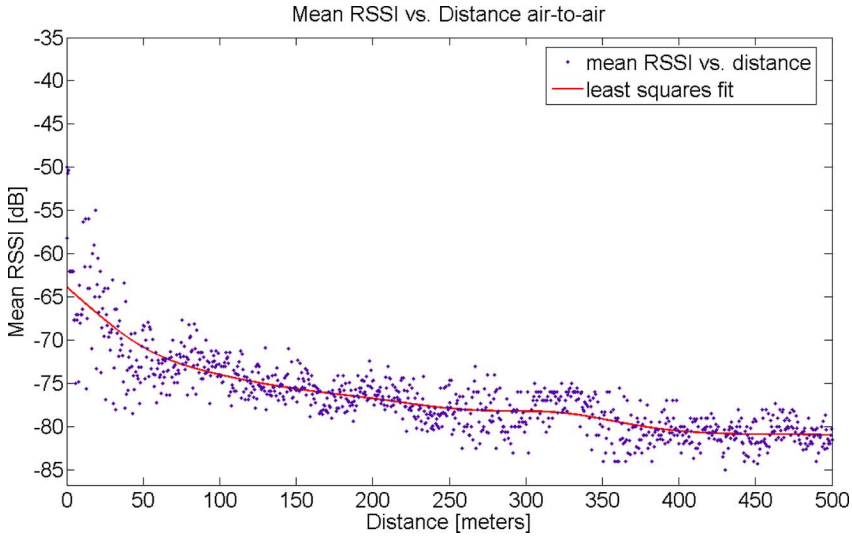

Fig. 20. Received signal strength (air-to-air) versus inter-vehicle separation.

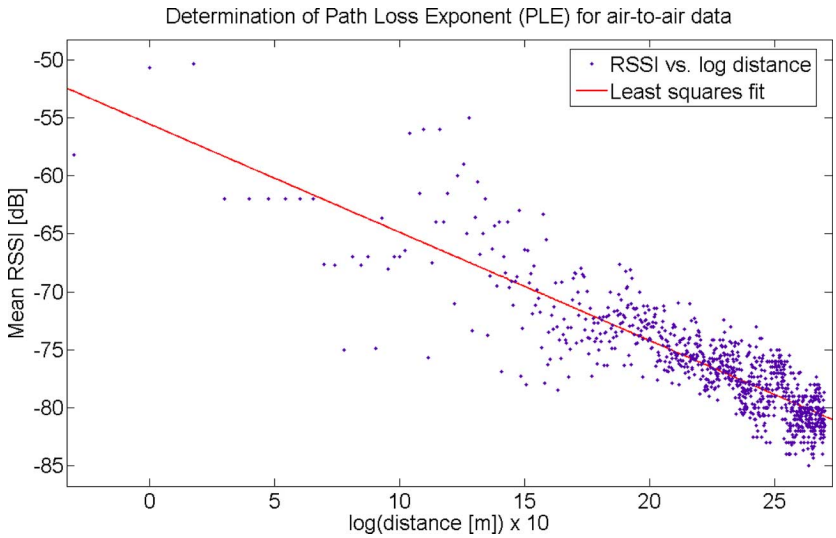

Fig. 21. Determination of path loss exponent using the plot of RSSI versus log of the inter-node separation (air-to-air). The slope of this plot, with its sign reversed, gives the value for the path loss exponent.

Similarly, the PLE for air-to-ground links was estimated to be 1.50. This difference in PLE clearly demonstrates that the signal strength drops off more rapidly in the air-to-ground links than in the air-to-air links.

As mentioned earlier, RSSI data and packet gap size data have limited usefulness near the limits of the communication range. It is, therefore, important to characterize the packet errors to obtain a more complete picture of the wireless transmission. Fig. 22 shows a bar chart detailing the number of packets successfully received and the number of packets dropped for various distances of the UAVs from the ground station. The number of packets dropped increase rapidly with distance and very few packets are successfully received beyond the distance of about 200 meters. This confirms the estimate for the communication range made earlier. The PER metric is calculated as the percentage of failed packets to the total number of packets transmitted. The plot for PER versus distance from the ground station is shown in Fig. 23. The PER curve is useful in characterizing the communication throughout its range. It shows how the error rate increases with increasing distance from the ground station. Based on the application, a cut-off point may be chosen as the effective range of communication. The maximum value that can be chosen for the smoothing length h is limited by the communication range experimentally determined above. If the smoothing length is chosen to be less than half the communication range, it would not affect the performance of the SPH algorithm. This is because the SPH algorithm does not care about vehicles that are more than $2h$ distance away. It may be reasoned that this is not a severe limitation when SPH acts to prevent collisions. However, communication range does limit the size of the goal region for a given number of vehicles in the swarm.

With this communication characterization information, an experiment was performed to measure the SPH control forces generated when two vehicles approached each other with varying speeds. The smoothing length for the kernel was set to 42 meters. The UAVs exchange data packets that contain information

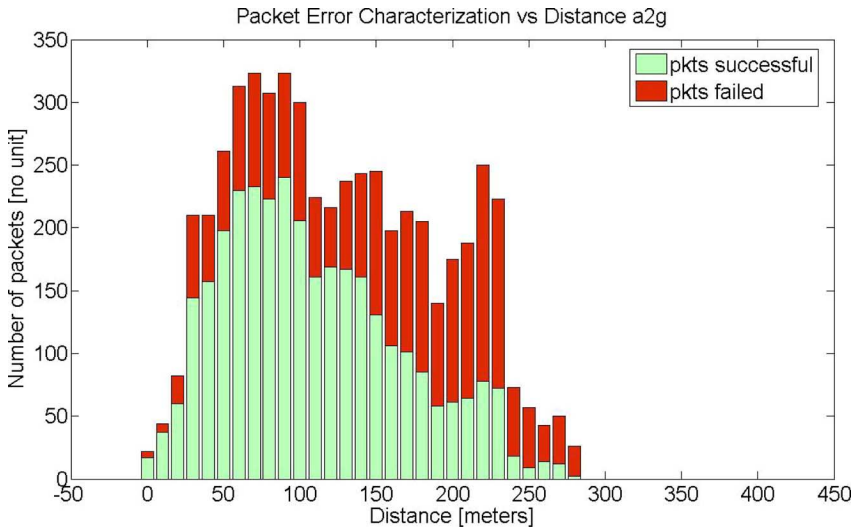

Fig. 22. Packets received and dropped versus distance. The successful packet counts are shown in light green color and the failed packet counts are in dark red.

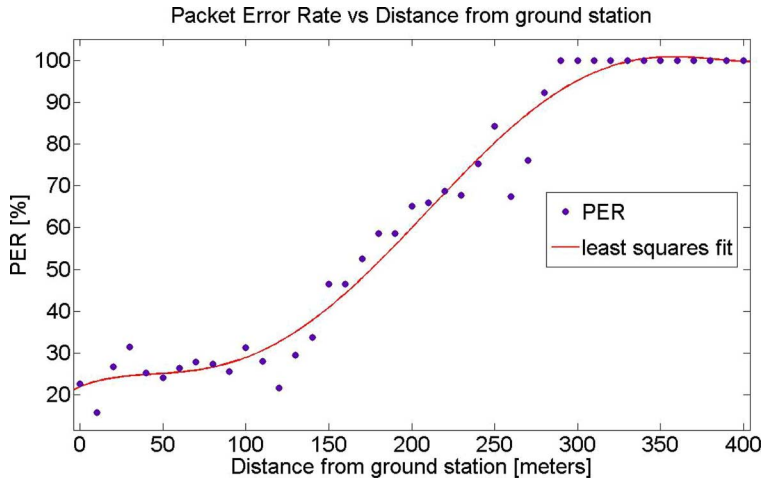

Fig. 23. Packet error rate (PER) versus distance grouped in bins of 10 meters. The PER values are shown as data points and the least squares fit is shown as a solid curve.

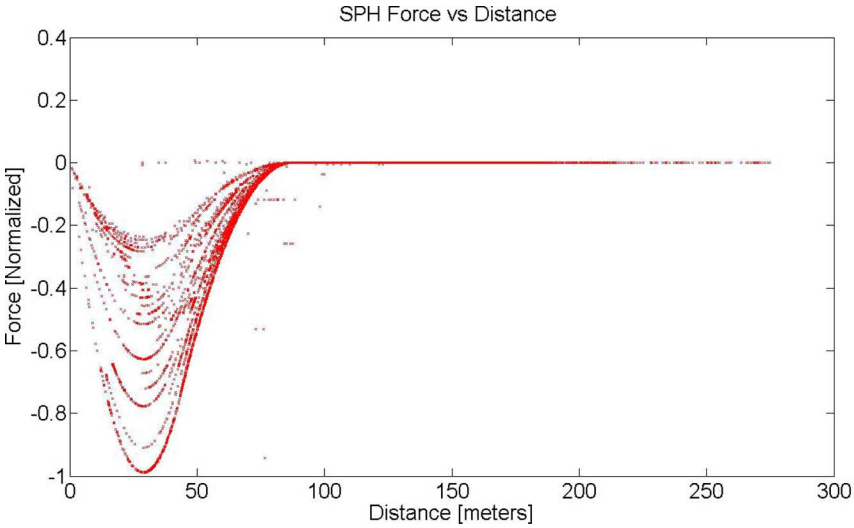

Fig. 24. Forces due to SPH vs the separation between the vehicles. Each sequence of data points that trace a spline-like curve, represent one pass of vehicle approaching each other with a certain relative velocity.

about their position, their hydrostatic pressure and their density. This data was used to compute a force based on SPH laws defined earlier. The plot for the SPH force as seen by one of the vehicles is shown in Fig. 24. It may be noted that the force due

to SPH is zero when the vehicles are separated by a distance greater than twice the smoothing length, h. The forces due to SPH are generated only when the vehicles are closer than twice the smoothing length. The forces are negative, which in our convention translates to a repulsive force. Thus, this force tends to push vehicles away from each other when they get too close. As the forces due to SPH are zero for vehicles that are far apart, it is not affected by vehicles that are outside the range of communication. The plot shows several values of SPH force generated based on the distance between the vehicles and their relative velocity of approach. Each sequence of data points that trace a spline-like curve, represent one pass of vehicle approaching each other with a certain relative velocity. In the experiment with three Delta-wing vehicles, the SPH forces caused the vehicles to maintain a uniform inter-vehicle separation within the loiter circle. The control gains were manually tuned to obtained faster convergence. The experiment uses a fixed value for the smoothing length, h, but a variable h could have been used, in the same way as it has been used in the simulations. The experiments allowed us to access the merits and demerits of the SPH controller in a typical real world application. It was seen that SPH algorithms could execute under stringent processing and memory constraints. It was demonstrated that it was computationally feasible to set up a SPH-based wireless network using low-powered Zigbee radios, controlled by the same 8-bit processor that executed the SPH-based control algorithm. The experiments reproduce the simulation results for multiple aerial vehicles in a circular loiter pattern. Further, the experiments may be seen to complement the simulation results obtained for the SPH-based controller, and provide useful information for setting up WSN applications.

IV. Conclusion

In this study, smoothed particle hydrodynamics (SPH) combined with vector field path following was used to control a group of UAVs. Several simulation runs in 3-D space were executed to investigate the different ways in which the SPH based controller could be used for a team of UAVs. The study assumes that the UAVs are 32 inch fixed wing aircrafts that move in 3-D space, maintaining a minimum velocity necessary to keep them afloat. The turning radius limitations for the UAVs are also taken into account in the 3-D simulations. Appropriate values for the smoothing length, h, and the control gains for optimal coverage were calculated as functions of the goal geometry, the number of vehicles and the desired airspeed that the vehicles needed to maintain. The circular, racetrack, and counter-rotating loiter patterns for vehicles in the goal region were studied. It was shown that the circulation component in the vector field does not have an effect on the h value required for equal spacing in the goal region. Simulation runs were conducted with additional virtual stationary SPH particles placed in the path of the moving vehicles, demonstrating the use of virtual SPH particles to model obstacles or adversarial regions. This mechanism allows the vehicles to dynamically change their paths when they sense an obstacle. The simulation used a variable smoothing length to control the inter-vehicle separation. This allowed the vehicles to travel in more densely packed groups when they were away from the goal region. Moreover, it was argued that adaptively changing the smoothing length could provide a mechanism to maintain uniform coverage in the goal region in the case of failure of one or more UAVs. SPH, therefore, was seen to provide several useful functionalities for the control of a swarm of UAVs at a low cost of computation. Finally, an experiment was conducted to create a simple wireless sensor network of UAVs using SPH for control. ZigBee radios, set to their lowest transmit power levels, were used for communication. The results of characterization of the air-to-air and air-to-ground communication links were presented. Received signal strength indicator (RSSI), path loss exponent (PLE), and packet error rate (PER) were used as metrics to characterize the wireless communication. The communication range imposes limitations on the maximum value of h, which, in turn, limits the size of the goal region for a given number of vehicles. The experiment demonstrated the viability of setting up a SPH-based wireless sensor networks of aerial vehicles, with minimal power and computational requirements. Moreover, the experiments highlighted an area of improvement. The use of vector path following along with the SPH algorithm results in a complex system with slightly increased computational loads. A SPH-only controller that works without the externally applied forces would further simplify the entire system. Our group has developed an SPH-only controller that obviates the need for the traditional vector path following algorithm, relying entirely on SPH for all control and navigation requirements. This will be the topic of a future publication. Summarizing, SPH methods provide very useful mechanisms for the control and co-ordination of a swarm of UAVs. The distributed nature of the computation allows it to be implemented on very basic on-board microprocessors, thereby reducing the overall cost of each unit. It fits in well with the vision of using a large number of small inexpensive UAVs to achieve mission-level autonomy in the performance of complex tasks.

References

[1] W. Pisano, D. Lawrence, and K. Mohseni, "Concentration gradient and information energy for decentralized uav control," in *AIAA Guidance, Navigation, and Control Conference and Exhibit*, Keystone, Colorado, Aug. 21–24, 2006, AIAA paper 2006-6459.

[2] D. Lawrence, E. Frew, and W. Pisano, "Lyapunov vector fields for autonomous unmanned aircraft flight control," *J. Guidance, Contr., . Dyn.*, vol. 31, no. 5, pp. 1220–1229, 2008.

[3] D. Lawrence, K. Mohseni, and R. Han, "Information energy for sensor-reactive UAV flock control," in *Proc. 3rd AIAA Unmanned Unlimited Techn. Conf., Workshop Exhibit*, Chicago, IL, Sep. 20–23, 2004, Paper 2004-6530.

[4] R. Beard, "Multiple uav cooperative search under collision avoidance and limited range communication constraints," in *IEEE CDC*, 2003, pp. 25–30.

[5] J. Allred, A. Hasan, B. Pisano, S. Panichsakul, P. Gray, R. Han, D. Lawrence, and K. Mohseni, "SensorFlock: A mobile system of networked micro-air vehicles," in *Proc. ACM SenSys 2007: 5th ACM Conf. Embedded Netw. Sens. Syst.*, Sydney, Australia, Nov. 6–9, 2007, pp. 117–129.

[6] J. J. Cione, E. W. Uhlhorn, G. Cascella, S. J. Majumdar, C. Sisko, N. Carrasco, M. D. Powell, P. Bale, G. Holland, P. Turlington, D. Fowler, C. W. Landsea, and C. L. Yuhas, "The first successful unmanned aerial system (uas) mission into a tropical cyclone (ophelia 2005)," in *Proc. AMS 12th Conf. IOAS-AOLS*, 2008, pp. 25–30.

[7] N. E. Leonard, D. A. Paley, F. Lekien, R. Sepulchre, D. M. Fratantoni, and R. E. Davis, "Collective motion, sensor networks, and ocean sampling," *Proc. IEEE*, vol. 95, no. 1, pp. 48–74, Jan. 2007.

[8] E. Fiorelli, N. Leonard, P. Bhatta, D. Paley, R. Bachmayer, and D. Fratantoni, "Multi-AUV control and adaptive sampling in Monterey bay," *IEEE J. Oceanic Eng.*, vol. 31, no. 4, pp. 935–948, Oct. 2006.
[9] J. Monaghan, "Smoothed particle hydrodynamics," *Ann. Rev. Astron. Astrophys.*, vol. 30, pp. 543–574, 1992.
[10] P. Berczik, "Modeling the star formation in galaxies using the Chemo-DynamicalSPH code," *Astrophys. Space Sci.*, vol. 271, no. 2, pp. 103–126, 2000.
[11] P. Cleary, J. Ha, V. Alguine, and T. Nguyen, "Flow modelling in casting processes," *Appl. Math. Modell.*, vol. 26, no. 2, pp. 171–190, 2002.
[12] P. Cleary, "Modelling confined multi-material heat and mass flows using sph," *Appl. Math. Modell.*, vol. 22, no. 12, pp. 981–993, 1998.
[13] R. M. L. C. A. Pimenta, M. L. Mendes, and G. Pereira, "Fluids in electrostatic fields: An analogy for multirobot control," *IEEE Trans. Magn.*, vol. 43, no. 4, pp. 1765–1768, Apr. 2007.
[14] L. Pimenta, N. Michael, R. Mesquita, G. Pereira, and V. Kumar, "Control of swarms based on hydrodynamic models," in *Proc. IEEE Int. Con. Robotics Autom.*, May 2008, pp. 1948–1953.
[15] S. Huhn and K. Mohseni, "Cooperative control of a team of AUVs using smoothed particle hydrodynamics with restricted communication," in *Proc. ASME 28th Int. Conf. Ocean, Offshore Arctic Eng.*, Honolulu, HI, May-Jun. 31–5, 2009, Paper OMAE 2009-79869.
[16] R. Beard, "Maximizing miniature aerial vehicles," *IEEE Robotics Autom. Mag.*, vol. 13, no. 6, pp. 34–43, 2006.
[17] S. Herbert, H. Tanner, V. Kumar, and K. Kyriakopoulos, "Closed loop motion planning and control for mobile robots in uncertain environments," in *Proc. 42nd IEEE Conf. Decision Contr.*, 2003, pp. 2926–2931.
[18] S. Li and W. Liu, *Meshfree Particle Methods*. New York: Springer Verlag, 2004.
[19] G. Lu, B. Krishnamachari, and C. Raghavendra, "Performance evaluation of the ieee 802.15.4 mac for low-rate low-power wireless networks," in *Workshop on Energy-Efficient Wireless Communications and Networks (EWCN '04), held in conjunction with the IEEE International Performance Computing and Communications Conference (IPCCC*, 2004, pp. 701–706.
[20] M. Petrova, J. Riihijarvi, P. Mahonen, and S. Labella, "Performance study of ieee 802.15.4 using measurements and simulations," in *Proc. IEEE Wireless Commun. Network. Conf.*, Apr. 2006, pp. 487–492.
[21] J. Zheng and M. Lee, *A Comprehensive Performance Study of IEEE 802.15.4*. Piscataway, NJ: IEEE Press, 2006, ch. 4, pp. 218–237.
[22] W. J. Pisano and D. A. Lawrence, "Autonomous uav control using a 3-sensor autopilot," in *Proc. AIAA Infotech Aerospace Conf.*, Rohnert Park, CA, May 2007.
[23] W. J. Pisano and D. A. Lawrence, "Autonomous gust insensitive aircraft," in *AIAA Guidance, Navigation Contr. Conf. Exhibit*, Honolulu, HI, Aug. 2008.
[24] T. Rappaport, *Wireless Communications: Principles and Practice*. Englewood Cliffs, NJ: Prentice Hall, 2001.

Apratim Shaw received the B.E. degree in mechanical engineering from the Birla Institute of Technology, Mesra, India, in 2001.

Currently, he is a graduate student in Aerospace Engineering Sciences at the University of Colorado at Boulder, which he joined in 2008. His research interests include mobile sensor networking, bio-inspired multi-robot systems, and adaptive control.

Kamran Mohseni (M'95) received the B.S. degree in mechanical engineering from the University of Science and Technology, Tehran, Iran, in 1990, the M.S. degree in aeronautics from the Imperial College of Science, Technology, and Medicine London, U.K., in 1993, and the Ph.D. degree in mechanical engineering from the California Institute of Technology (Caltech), Pasadena, in 2000.

Currently, he is an Associate Professor in Aerospace Engineering Sciences at the University of Colorado at Boulder, which he joined in 2001 after a year as a Postdoctoral Fellow in Control and Dynamical Systems at Caltech. His research interests are in mobile sensor networking, sensor platform development, and bio-locomotion.

Dr. Mohseni is a member of the American Society of Mechanical Engineers (ASME), the American Physical Society (APS), the Society for Industrial and Applied Mathematics (SIAM), and an Associate Fellow of the American Institute of Aeronautics and Astronautics (AIAA).